Glass-Forming Ability of Soda Lime Borate Liquids

Zheng, Qiuju; Mauro, J.C.; Smedskjær, Morten Mattrup; Youngman, R.E.; Potuzak, M.; Yue, Yuanzheng

Published in:
Journal of Non-Crystalline Solids

DOI (link to publication from Publisher):
10.1016/j.jnoncrysol.2011.11.004

Publication date:
2012

Document Version
Early version, also known as pre-print

Journal of Non-Crystalline Solids 358 (2012) 658–665

Contents lists available at SciVerse ScienceDirect

Journal of Non-Crystalline Solids

journal homepage: www.elsevier.com/ locate/ jnoncrysol

Glass-forming ability of soda lime borate liquids

Qiuju Zheng [a,b], John C. Mauro [b,*], Morten M. Smedskjaer [b], Randall E. Youngman [b], Marcel Potuzak [b], Yuanzheng Yue [a,c,**]

[a] Section of Chemistry, Aalborg University, DK-9000 Aalborg, Denmark
[b] Science and Technology Division, Corning Incorporated, Corning, 14831 NY, USA
[c] Key Laboratory of Glass and Ceramics, Shandong Polytechnic University, Jinan 250353, China

ARTICLE INFO

Article history:
Received 22 September 2011
Received in revised form 3 November 2011
Available online 28 November 2011

Keywords:
Glass-forming ability;
Glass stability;
Soda lime borate glasses;
Fragility;
Boron speciation

ABSTRACT

We investigate the composition dependence of glass-forming ability (GFA) of a series of iron-containing soda lime borate liquids by substituting Na_2O for B_2O_3. We have characterized GFA by measuring the glass stability against crystallization using a differential scanning calorimeter (DSC). The results show that the GFA decreases when substituting Na_2O for B_2O_3. Moreover, we find that there is no direct link between the kinetic fragility and GFA for the soda lime borate series studied herein. We have also discovered and clarified a striking thermal history dependence of the glass stability against crystallization. In particular, the two glasses containing 20 and 25 Na_2O mol% do not exhibit crystallization exotherms during the second DSC upscan at 10 and 20 K/min following prior slow (10 and 20 K/min) downscans. This indicates that the glass stability of these compositions can be enhanced by cooling their melts to the glassy state slowly, before any reheating. We explain this phenomenon in terms of the thermal history dependence of boron speciation.

1. Introduction

Inorganic glasses are predominantly produced using the melt-quenching technique, where the batch materials are heated to a temperature above the liquidus temperature and then cooled sufficiently fast to avoid crystallization [1–3]. In order to optimize the glass production process, it is important to know the glass-forming ability (GFA) of the melt. The GFA has been systematically investigated for a range of silicate [4], aluminosilicate [5], borosilicate [6], alkali borate [7], and alkaline earth borate [6] liquids. Traditionally borate glasses have found only limited applications due to their poor chemical durability, but recently it has been found that borate glass nanofibers are bioactive and promote the healing of flesh wounds [8]. Hence, it has become increasingly important to understand the GFA of more complex borate liquids. To the best of our knowledge, the GFA of alkali alkaline earth borate liquids has not received much attention. Moreover, the so-called boron anomaly makes the structural foundation of borate glass and liquid properties especially interesting. In borate compositions, the initial addition of alkali or alkaline earth oxides affects properties differently compared to further additions of these same modifiers due to conversion of boron between three-fold (trigonal) coordination and four-fold (tetrahedral) coordination [9]. Hence, the effect could also cause an "anomalous" composition dependence of GFA, and it may thus be particularly interesting to explore this effect [7,9,10]. In this paper, we therefore attempt to quantify and understand the GFA of a series of soda lime borate compositions and connect these results back to general features of glass formation in inorganic liquids.

GFA is a measure of how easily a melt is vitrified and can be quantified by determining the critical cooling rate q_c [1], which is defined as the minimum cooling rate required to vitrify a melt, i.e., to obtain a glass with a crystal concentration lower than a certain standard value such as 1 ppm. However, it is difficult and time-consuming to determine q_c precisely, and therefore alternative methods for quantifying GFA have been developed. For example, various glass stability (GS) parameters have been proposed [6,11]. Generally speaking, these parameters all describe the ability of a glass to bypass crystallization upon heating. It has been found that GFA and GS parameters have a direct relationship [4,5], i.e., GS increases with increasing GFA. While there are several proposed metrics for GS, the Hruby parameter (K_H) shows a better correlation with GFA compared with other parameters [12]. Therefore, we use K_H as a measure of GFA in this work. K_H can be calculated from three characteristic temperatures:

$$K_H = \frac{T_c - T_g}{T_m - T_c}, \quad (1)$$

where T_g is the onset glass transition temperature, and T_c and T_m are the onset temperatures of the crystallization peak and the melting peak during heating. A high value of K_H indicates high glass stability. These characteristic temperatures can be determined experimentally using

* Corresponding author. Tel.: +1 607 974 2185; fax: +1 607 974 2410.
** Corresponding author. Tel.: +45 99408522; fax: +45 9635 0558.
E-mail addresses: mauroj@corning.com (J.C. Mauro), yy@bio.aau.dk (Y.Z. Yue).

0022-3093/$ – see front matter © 2011 Elsevier B.V. All rights reserved.
doi:10.1016/j.jnoncrysol.2011.11.004

differential scanning calorimetry (DSC). A typical DSC curve for a glass exhibiting high tendency for crystallization has three well-defined characteristic peaks upon heating: an endothermic glass transition peak, an exothermic crystallization peak, and an endothermic melting peak (Fig. 1). T_g, T_c, and T_m are the onset temperatures of these three peaks, which are determined as the intersection of tangents to the curve, traced on the baseline and on the peak side (Fig. 1). This method is called the "tangent method" [13] and it has its limitations due to the uncertainty in drawing tangents along the sides of the DSC peaks. The inherent drawbacks of using the GS parameters such as K_H are discussed later in this paper.

Shear viscosity of glass-forming liquids is an important temperature-dependent property governing glass formation [14]. It is also related to the GFA, since the flow behavior determines the kinetic activation barriers for both nucleation and crystal growth [6]. Several models have been proposed for describing the temperature dependence of the viscosity (η) of a melt, e.g., Vogel–Fulcher–Tammann (VFT) [15] and Avramov–Milchev (AM) [16]. However, these models exhibit systematic error when extrapolating to low temperatures as described elsewhere [17]. Recently, based on energy landscape analysis and the temperature-dependent constraint model for configurational entropy [18–20], Mauro et al. have derived a new three-parameter viscosity model [17]:

$$\log \eta = \log \eta_\infty + \frac{K}{T}\exp\left(\frac{C}{T}\right) \tag{2}$$

where η_∞ is the high-temperature viscosity limit and K and C are constants. This model has been shown to provide improved fitting quality of measured viscosity–temperature curves compared to the existing models. Furthermore, it provides a physically realistic description of liquid dynamics across the full range of temperatures [17,21]. Based on the analysis in [17,21], it has been concluded that η_∞ is a universal composition-independent constant equal to approximately 10^{-3} Pa s. Since the viscosity at T_g (η_{Tg}) is equal to 10^{12} Pa s for oxide glasses [22], $\log \eta_{Tg} - \log \eta_\infty = 12 - (-3) = 15$. Eq. (2) can then be expressed in terms of the liquid fragility index m and T_g:

$$\log_{10}\eta(T) = -3 + 15\frac{T_g}{T}\exp\left[\left(\frac{m}{15}-1\right)\left(\frac{T_g}{T}-1\right)\right]. \tag{3}$$

The definition of the fragility m is due to Angell [3], who noted that liquids can be classified as either "strong" or "fragile" depending on whether they exhibit an Arrhenius or super-Arrhenius scaling of viscosity with temperature, respectively. The slope of the Angell curve ($\log \eta$ as a function of T_g scaled inverse temperature (T_g/T)) at

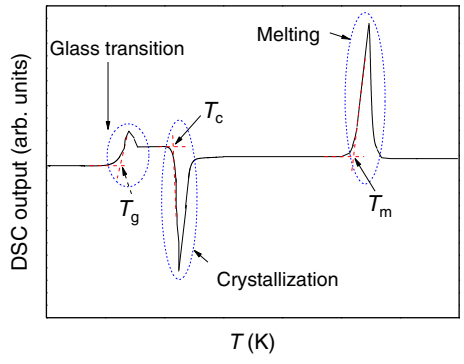

Fig. 1. Typical DSC curve of a glass that easily crystallizes during heating. The procedure for determining the three characteristic temperatures T_g ,T_c and T_m is illustrated.

T_g defines the fragility index,

$$m = \frac{\partial \log_{10}\eta}{\partial\left(T_g/T\right)}\Big|_{T=T_g}. \tag{4}$$

An inverse correlation between fragility index and GFA has been found for various metallic glass-forming liquids in addition to some silicate liquids [23,24]. "Strong" melts have a more consistently rigid structure upon temperature changes compared to "fragile" melts. This rigidity could create steric hindrance towards crystallization during cooling, and therefore strong melts are expected to have better GFA. However, it remains unknown if and how the fragility of borate liquids is correlated with their GFA. Clarifying this relation is one of the objectives of the current study, where we characterize the GFA of these systems by determining their crystallization tendency and viscous flow behavior. We also demonstrate a dramatic enhancement of the glass stability against crystallization for two of the high-Na_2O compositions under study after imposing a new thermal history on these glasses. Finally, we discuss the possible structural origin of the enhancement of glass stability.

2. Experiments

2.1. Sample preparation

Eight glass samples were synthesized using analytical reagent-grade H_3BO_3 (Sigma-Aldrich, ≥99.5%), Na_2CO_3 (Sigma-Aldrich, ≥99.5%), $CaCO_3$ (Fluka, ≥99%), and Fe_2O_3 (Aldrich, ≥99.9%) powders. Seven of them have the compositions (mol%) of $x$$Na_2O$-10CaO-(89-$x$)$B_2O_3-1Fe_2O_3$ with $x = 5$, 10, 15, 20, 25, 30, and 35. The eighth glass has a composition (mol%) of 25Na_2O-10CaO-65B_2O_3 (denoted B-Na25). The thoroughly mixed batches were melted in a covered $Pt_{90}Rh_{10}$ crucible at 1323–1423 K for ~15 min in an inductively heated furnace. Melting by using a covered crucible and the relatively low melting temperatures and short times were chosen to minimize boron evaporation, and homogeneity was ensured by the convection currents created in the melt due to the induction furnace. In order to obtain glasses, the melts were cast onto a brass plate and cooled in air to room temperature. Measurements of the weight loss due to melting indicate that the glasses are within 1–2 wt.% of the desired compositions [25].

Owing to the hygroscopic character of the borate glasses, all samples were kept in glass or plastic containers with desiccant. All of the glasses under study besides B-Na25 contain 1 mol% Fe_2O_3, since they have also been used in a parallel study that established the influence of boron speciation on ionic transport [26]. The transport properties were studied using an inward cationic diffusion approach, which requires the presence of a polyvalent element in the glass [27]. Moreover, the structure and topology of these glasses have been studied in [25].

2.2. DSC measurements

For the glass stability investigations, the three characteristic temperatures (T_g, T_c, and T_m) were determined using a calorimetric method as shown in Fig. 1. The differential scanning calorimetry (DSC) measurements were performed with a simultaneous thermal analyzer (STA 449 C Jupiter, Netzsch, Selb, Germany) at a rate of 20 K/min for both up- and downscanning in a purged argon atmosphere. The samples were heated to 1273 K to locate the glass transition, crystallization, and melting peaks. As mentioned earlier, the characteristic temperatures were determined using the "tangent method". This method has uncertainties of approximately ±2 to 3 K.

In order to obtain the heat capacity curves of the standard glass (cooling and heating at 10 K/min), the samples were subjected to two runs of DSC upscans and downscans. The rates of the upscans

and downscans were always equal to 10 K/min. The recorded heat flow of the first upscan reflects the enthalpy response of a sample with an unknown thermal history (i.e., an unknown cooling rate experienced by the sample during melt-quenching), whereas that of the second upscan reflects the enthalpy response of the sample with a well-defined thermal history (i.e., a known cooling rate). The standard T_g is determined from the second upscan curve as the onset temperature of the glass transition peak [28]. The isobaric heat capacity (C_p) curve for each measurement was calculated relative to the C_p curve of a sapphire reference material of comparable mass.

2.3. Viscosity measurements

In order to determine the liquid fragility index, viscosity measurements were performed. The low viscosities (approximately 10^0–10^3 Pa s) were measured using a concentric cylinder viscometer. The viscometer consisted of four parts: furnace, viscometer head, spindle, and sample crucible. The viscometer head (Physica Rheolab MC1, Paar Physica) was mounted on top of a high temperature furnace (HT 7, Scandiaovnen A/S). Spindle and crucible were made of $Pt_{80}Rh_{20}$. The viscometer was calibrated using the National Bureau of Standards (NBS) 710A standard glass. In the high viscosity range (approximately 10^{10}–10^{13} Pa s), the viscosity was measured using micro-penetration viscometry with a vertical dilatometer (Model VIS 405, Bähr-Termoanalyse, Hüllhorst, Germany). The precision of the equipment was tested using the Deutsche Glastechnische Gesellshaft (DGG) standard glass I and was found to be within ±1% of the standard linear viscosities stated in [29]. The viscosity of the $x=35$ composition could not be measured due to its high tendency for crystallization.

2.4. ^{11}B MAS NMR spectroscopy

Boron speciation in glasses depends on thermal history [30]. In order to investigate the thermal history dependence of boron speciation and how it affects GFA of the soda-lime borate liquids, we carried out ^{11}B magic angle spinning (MAS) NMR measurements on selected samples. The NMR spectra were collected at 11.7 T (160.34 MHz resonance frequency) using a 2.5 mm MAS NMR probe and sample spinning at 20 kHz. The data were acquired using a short (π/12) pulse width of 0.6 μs and 1 s recycle delays. 600 scans were collected; data were processed without line broadening and referenced to an external aqueous boric acid sample (19.6 ppm from BF_3-Et_2O).

^{11}B MAS NMR spectra were fit using DMFit [31], with two trigonal and two tetrahedral lineshapes for each spectrum. The trigonal sites were reproduced using second-order quadrupolar broadened lineshapes, and a mixture of Gaussian and Lorentzian lineshapes was sufficient to fit the 4-fold coordinated boron resonances. The experimental data required at least two distinct 3-fold coordinate boron peaks and one 4-fold coordinated boron resonance. A second 4-fold coordinated peak was added to the simulations to account for minor peak intensity to the higher-shielded side of the 4-fold coordinated boron resonance. Regardless of the exact number of distinct sites in these glasses, all data were fit using identical methods and thus uncertainties in the fraction of tetrahedral to total boron (N_4) are on the order of ±0.2%.

2.5. XRD measurements

The resulting crystalline phases after the first DSC scan were determined from X-ray diffraction (XRD) measurements. The quantitative XRD analyses were performed using a PANalytical CUBIX PRO instrument. XRD signals were recorded in the range $5°<2\theta<65°$ with a stepsize of 0.02 and a steptime of 120 sec/step. The X-rays were generated by a Cu Kα target operated at 40 kV and 45 mA. 10 wt.% TiO_2 was added as internal standard by mixing in a Herzog disk mill twice for 30 s each.

3. Results

DSC upscans are performed on the borate glass series at a heating rate of 20 K/min to determine the glass stability upon heating. Fig. 2 shows the temperature dependence of the DSC output (in arbitrary units) for the seven glasses. The first endothermic peak is attributed to the glass transition. For the four glasses with $x=20$, 25, 30, and 35, there is an exothermic peak well above T_g, which is attributed to crystallization of the glass. An endothermic crystal melting peak occurs following the crystallization peak [13]. No crystallization peak is observed for the three glasses with $x=5$, 10, and 15 during dynamic heating at 20 K/min and therefore K_H cannot be calculated for those glasses. This implies that these compositions have higher glass stability than the other compositions [24]. The determined values of T_g, T_c, and T_m and the Hruby parameter K_H [12] are stated in Table 1.

It has been found that GFA and kinetic fragility have an inverse correlation for some glass-forming systems [23,24]. Here the question is whether this inverse relation exists for the soda lime borate liquid series. Fragility is traditionally determined from viscosity measurements to obtain the kinetic fragility index m. Besides determining m, we also determine the thermodynamic values, which are associated with thermodynamic fragility for many glass systems, such as the jump in isobaric heat capacity (C_p) in the glass transition region [3,32–34] and glass transition width (ΔT_g) [35]. Therefore, another question is whether there is a parallel relation between the kinetic and the thermodynamic fragilities.

The temperature dependence of viscosity obtained from both micro-penetration and concentric cylinder viscometry is illustrated by the Angell plot in Fig. 3. The experimental data are fitted to Eq. (3) [17], and the kinetic fragility (m) is derived from the best-fit of Eq. (3) (see Table 1). We find that m increases with increasing concentration of Na_2O, but after reaching its maximum value at $x=25$, it starts to decrease. For the thermodynamic fragility, we determine the C_p jump as $C_{pl}-C_{pg}$, where C_{pg} and C_{pl} are the isobaric heat capacities for the glass at T_g and the liquid, respectively, as shown in Fig. 4. C_{pl} is determined as the offset value of the C_p overshoot above the glass transition range. Another characteristic value is the overshoot value of the glass transition peak, $C_{p.peak}$. It should be noted that this peak value is not the intrinsic heat capacity of the glass at the peak temperature; instead it is a reflection of the kinetic consequence of the glass transition during upscanning. The glass transition width (ΔT_g) is determined as $T_{g\cdot offset}-T_g$, where $T_{g\cdot offset}$ is the temperature at the offset

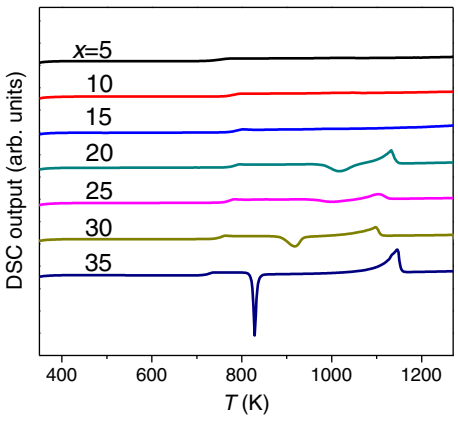

Fig. 2. DSC output (arbitrary units) versus temperature (T) during heating at 20 K/min for the glasses with compositions of $x$$Na_2O$–10CaO–(89-$x$)$B_2O_3$–1$Fe_2O_3$.

Table 1
Characteristic temperatures, K_H, N_4 [25], NBO/B, and m of the seven glasses ($x$$Na_2O$-10CaO-(89-$x$)$B_2O_3-1Fe_2O_3$). The errors in the characteristic temperatures are approximately ±2-3 K and uncertainties in N_4 are on the order of ±0.2%.

Sample (x=)	T_g (K)	T_c (K)	T_m (K)	K_H	N_4 [at%]	NBO/B	m
5	728	n/a	n/a	n/a	16	0.197	49±1
10	764	n/a	n/a	n/a	24	0.266	59±1
15	774	n/a	n/a	n/a	36	0.316	63±1
20	772	979	1062	2.49	40	0.47	67±2
25	760	954	1055	1.92	46	0.634	74±1
30	742	887	978	1.59	43	0.926	65±2
35	715	824	1118	0.37	42	1.247	n/a

of the C_p overshoot. The procedures for determining C_{pl}, C_{pg}, $C_{p.peak}$, and ΔT_g are illustrated in the inset of Fig. 4.

The composition dependencies of the values of C_{pl}–C_{pg}, $C_{p.peak}$–C_{pg}, and ΔT_g are shown in Figs. 5–7, respectively. It can be seen that there is no apparent trend in C_{pl}–C_{pg} with composition (Fig. 5), yet there is a trend in $C_{p.peak}$–C_{pg} and ΔT_g with composition (Fig. 6). The kinetic fragility (quantified by m) shows a positive correlation with the values of $C_{p.peak}$–C_{pg} and the glass transition width, which are in this work regarded as indirect measures of the thermodynamic fragility. This is expected because fragility is fundamentally a kinetic property, and the glass transition width is a reflection of kinetics (i.e., a steeper viscosity curves gives a more sudden breakdown of ergodicity [35,37] at T_g). But $C_{pl}-C_{pg}$ is a purely thermodynamic quantity, and the connection to kinetic fragility is apparently lost for these borate glasses. In Section 4.2, we will discuss whether there is a correlation between fragility and GFA.

Interestingly, two of the glasses under study (with $x=20$ and 25) do not exhibit any crystallization exotherms during the second DSC upscan at 20 K/min to 1273 K when they have been subjected to a prior upscan to 1273 K at 20 K/min and a subsequent downscan at the same rate. The DSC curves for the glass with $x=20$ are shown in Fig. 8(a). The same phenomenon is also observed when the second upscan rate is lowered to 10 K/min (Fig. 8(b)). This means that the stability of these two glasses against crystallization is dramatically enhanced after they undergo a slow cooling process. The enhancement of the glass stability can also be observed in glasses containing higher Na_2O content, e.g. glasses with $x=30$ and 35 as shown in Fig. 9. The glass with $x=30$ shows a crystallization peak during the first downscan at 20 K/min. This implies that the cooling rate is lower than the critical cooling rate, and hence the melt crystallizes during cooling. After cooling, the sample contains both glass and crystal phases. In the second upscan, there is no crystallization peak, indicating that the remaining glass phase does not crystallize during the second upscan. In other words, the GS of the remaining glass is enhanced after the first downscan. The glass with $x=35$ shows similar behavior to that with $x=30$.

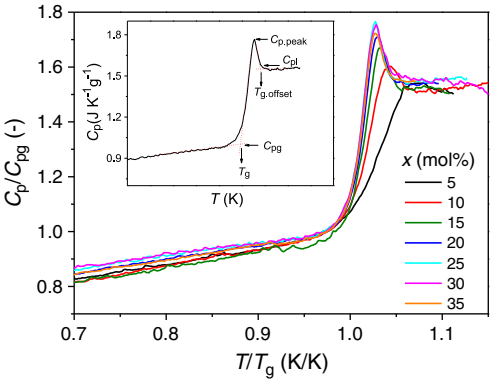

Fig. 4. Glass transition of the glasses ($x$$Na_2O$–10CaO–(89-$x$)$B_2O_3$–1$Fe_2O_3$) determined by DSC at a heating rate of 10 K/min subsequent to a cooling rate of 10 K/min. The plots are shown as the isobaric heat capacity (C_p) divided by C_p at T_g ($C_p/C_p(T_g)$) against T/T_g.

We have also determined the crystal phases of the sample with $x=20$ resulting from the first DSC upscan. This was done by conducting X-ray diffraction (XRD) measurements on samples that were heated in a muffle furnace by using the same conditions as during the DSC scan. As shown in Fig. 10, the sample that has been heat treated contains both crystalline and glassy phases. Using the Rietveld refinement method with an internal standard, the amounts of crystalline and glassy phase are determined to be 56 and 44 wt.%, respectively. The main crystalline phase (97.7 wt.%) is calcium sodium pentaborate, which consists of complex metaborate sheets with a B_5O_9 building block. The B_5O_9 unit contains BO_4 and BO_3 groups in the ratio of 2:3 in two rings, and Na and Ca are partially ordered in sites in channels between the metaborate sheets [38]. There are also two other low concentration crystals: boron oxide (2.0 wt.%) and iron boride (0.3 wt.%).

4. Discussion

4.1. Glass stability

Fig. 11 (a) shows the Hruby parameter (K_H) as a function of Na_2O concentration (x) for the four glasses with $x=20$, 25, 30, and 35. In general, the GFA decreases with increasing substitution of Na_2O for

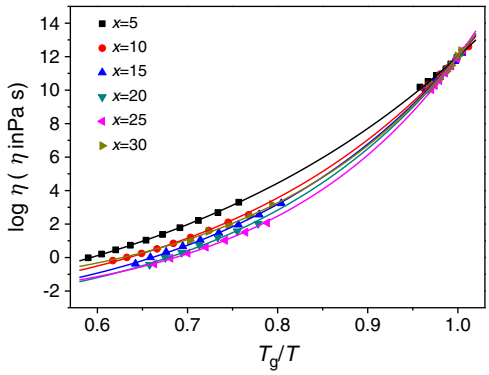

Fig. 3. Angell fragility plot showing the logarithmic viscosity ($\log\eta$) as a function of the T_g scaled inverse temperature (T_g/T) for the glasses with compositions of $x$$Na_2O$–10CaO–(89-$x$)$B_2O_3$–1$Fe_2O_3$.The error ranges for the high viscosity measurements (by the micro-penetration method) and for the low viscosity measurements (by the concentric cylinder method) were $\Delta\log\eta=\pm0.06$ and ±0.02 (η in Pa s), respectively [36].

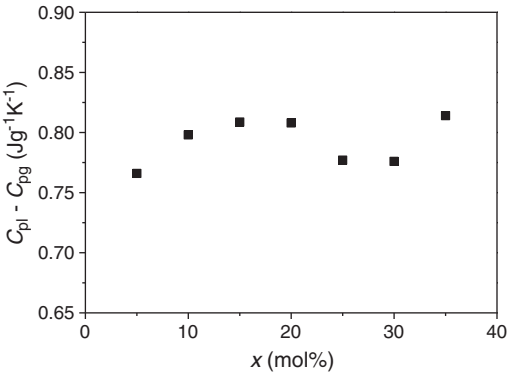

Fig. 5. The step change in the heat capacity (C_{pl}–C_{pg}) at the glass transition as a function of Na_2O content (x) for the seven glasses ($x$$Na_2O$–10CaO–(89-$x$)$B_2O_3$–1$Fe_2O_3$). The step change is determined as $C_{pl}-C_{pg}$, where C_{pg} is the isobaric heat capacity of the glass at T_g and C_{pl} is the isobaric heat capacity of the liquid, which is determined as the offset value of the C_p overshoot above the glass transition range. The uncertainties in $C_{pl}-C_{pg}$ are on the order of ±2–3%.

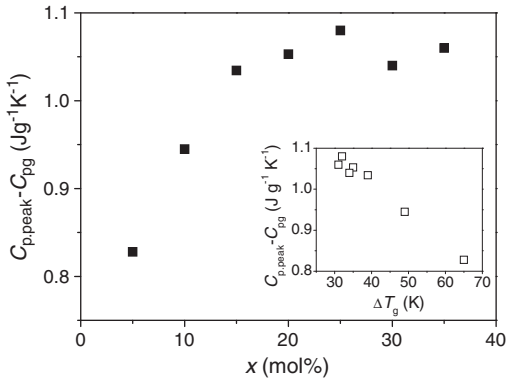

Fig. 6. $C_{p.peak}$–C_{pg} as a function of the Na_2O content (x) for the glasses ($x$$Na_2O$–10CaO–(89-$x$)$B_2O_3$–1$Fe_2O_3$), where $C_{p.peak}$ is the heat capacity value of the C_p overshoot peak. Inset: $C_{p.peak}$-C_{pg} as a function of the glass transition width (ΔT_g) during heating. The uncertainties in $C_{p.peak}$–C_{pg} are on the order of ±2-3%.

B_2O_3. To understand this trend, the fractions of tetrahedral boron to total (N_4) and NBO/B are determined and listed in Table 1, where NBO/B is the average number of non-bridging oxygens per boron tetrahedron or triangle. With the values of N_4, we are able to calculate the number of NBOs per boron. The boron itself can be tetrahedral or trigonal. As shown in Table 1, K_H decreases as the NBO/B increases for x = 20, 25, 30, and 35. The K_H values of glasses with x = 5, 10, and 15 are unknown higher values, but we suppose that the GFA increases as the value x decreases, i.e., NBO/B decreases. An increase of NBO/B lowers the connectivity of the network, which creates escape channels for the moving particles [39]. Consequently it is easy for the particles to rearrange, and hence there may be a greater tendency for crystallization. However, following Phillips–Thorpe constraint theory, we note that a sufficiently low value of NBO/B would also promote crystallization, since rigid structures would then easily percolate throughout the system resulting in crystallization [19,20].

Fig. 11(b) shows N_4 and NBO/B as a function of Na_2O concentration for all seven glasses. The results indicate that the GFA is closely related to the degree of network connectivity [19]. Boron speciation also has a direct influence on the connectivity. However, N_4 does not show a direct relation with K_H. There is apparently an influence of both NBO/B and N_4 on GFA, since both of these parameters affect the degree of network connectivity. This indicates that when comparing two glasses with different amounts of network former, NBO/B plays a determining role in controlling GFA, while the boron speciation plays a less important role. However, when comparing two glasses with the same amount of network former, the N_4 will play an important role, as will be discussed in Section 4.3.

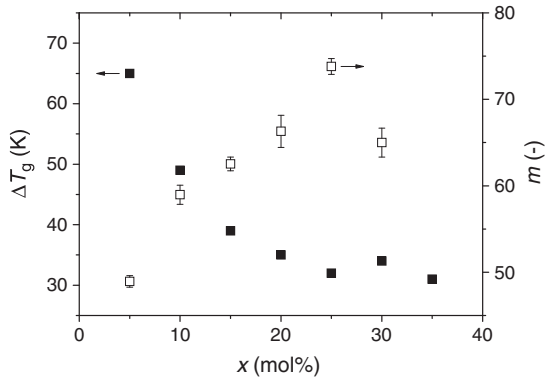

Fig. 7. Glass transition width (ΔT_g) and liquid fragility index (m) as a function of the Na_2O content (x) for the glasses ($x$$Na_2O$–10CaO–(89-$x$)$B_2O_3$–1$Fe_2O_3$). ΔT_g is determined as $T_{g\text{-offset}} - T_g$, where $T_{g\text{-offset}}$ is the temperature at the offset of the C_p overshoot. The errors in ΔT_g are approximately ±2-3 K.

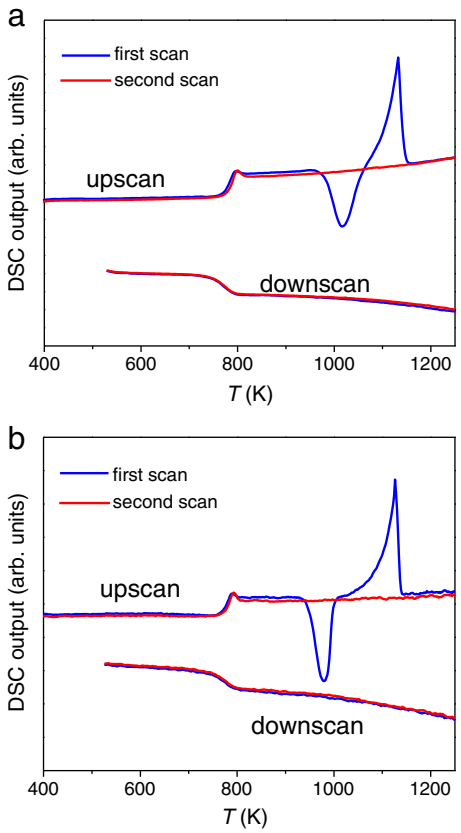

Fig. 8. DSC scans for the glass with x = 20 using (a) 20 K/min heating and cooling and (b) 10 K/min heating and cooling.

For three of the glasses under study, the Hruby parameter could not be determined, since no crystallization was observed during heating at the applied rates (10 and 20 K/min). It should be noted that the phase transitions observed during a DSC scan are dynamic, i.e., the characteristic temperatures are dependent on the heating rate employed during the measurements. Especially for glasses with high stability (e.g., x = 5, 10, 15), the crystallization and melting processes can be bypassed when using a sufficiently high heating rate. For good glass formers, K_H cannot be determined using the accessible heating rates of a DSC since no crystallization peak is observed. However, theoretically K_H must have a finite value that could be determined using a sufficiently low heating rate beyond the DSC heating rate window. This highlights the limitation of the Hruby parameter with the current DSC techniques. Actually there are several other GS parameters, e.g. K_T, K_W, K_{LL} [4,5], which all use the same characteristic

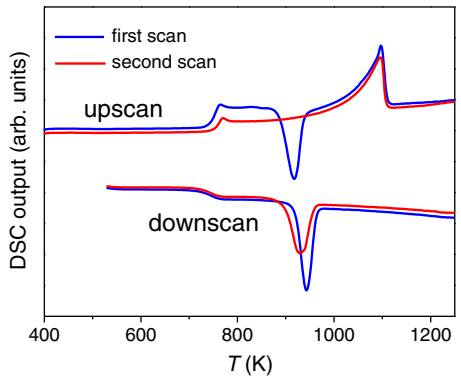

Fig. 9. DSC scans for the glass with x = 30 at 20 K/min heating and cooling.

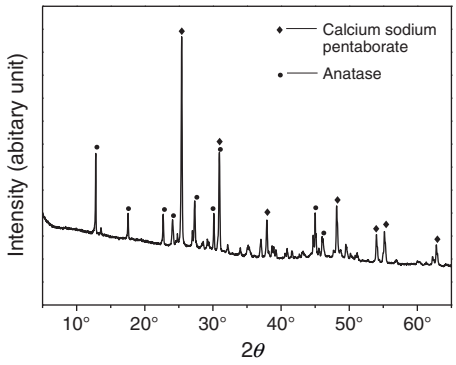

Fig. 10. X-ray diffraction (XRD) pattern of the glass with $x=20$ after crystallization resulting from the first DSC upscan. 10 wt.% of crystalline anatase has been added as an internal standard. The intensities of anatase signals were then used to quantify the amount of the other crystalline phases.

temperatures, i.e., T_g, T_c, and T_m. Here, we have only shown the results of the representative Hruby parameter, since the other parameters show similar trends. However, the inherent limitations of the Hruby parameter represent a universal drawback for any GS parameter, which includes characteristic temperatures. Therefore, a more universal GFA parameter which can be applied to any glass-forming liquid is needed.

4.2. Relationship between Fragility and GFA

In our attempt to understand the composition dependence of GFA for soda lime borate liquids, we will investigate the possible correlation between fragility and GFA. However, for this correlation to be insightful, it is important first to understand the composition

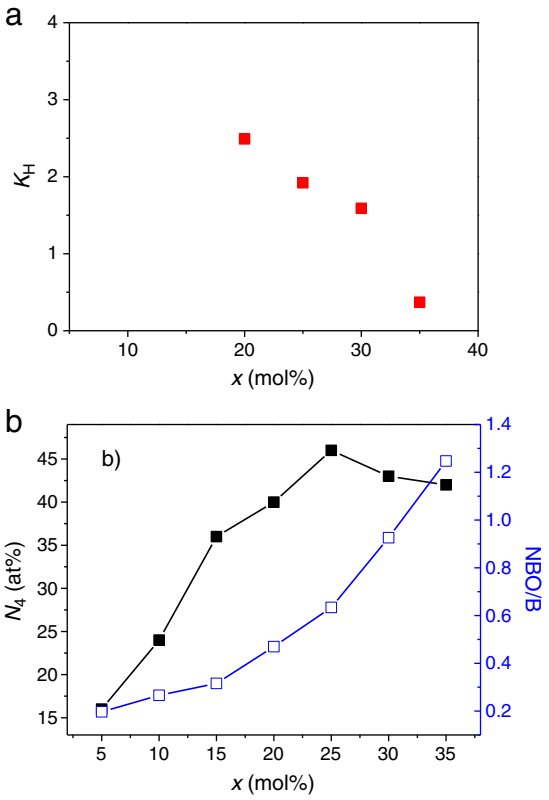

Fig. 11. (a) Hruby parameter (K_H) as a function of the Na_2O content (x) for the four glasses with $x=20$, 25, 30, and 35. (b) N_4 and NBO/B as a function of x. The uncertainties in N_4 are on the order of $\pm 0.2\%$ and the errors in K_H are around ± 0.03.

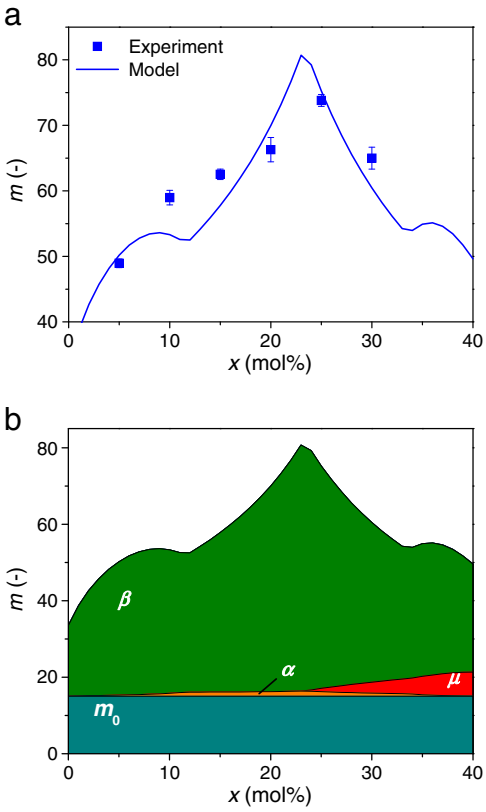

Fig. 12. (a) Dependence of fragility (m) on the Na_2O content (x) for the glasses ($x$$Na_2O$–10CaO–(89-$x$)$B_2O_3$–1$Fe_2O_3$). The solid line shows the predicted composition dependence of m using a topological model [25]. (b) Contribution of each type of topological constraint to the calculated fragility. m_0 is defined as the fragility index of the theoretically strongest liquid, and found to be 15 from Eq. (4).

dependence of fragility. We obtain this understanding from topological constraint theory [19,20], since Gupta and Mauro [9,18] have developed a new topological modeling approach that enables accurate prediction of the scaling of both glass transition temperature and fragility with composition. A key feature of the approach is the incorporation of temperature-dependent constraints that become rigid as a liquid is cooled. Recently, Smedskjaer et al. have extended the topological modeling approach to soda-lime borate systems [25]. The basic three steps to apply the topological modeling approach are: (1) identify and count the number of distinct network forming species (i.e., BO_4, BO_3, O, and M^{NB} (network modifiers (Na and Ca) that create NBOs); (2) identify and count the number of constraints associated with each species; and (3) calculate fragility in terms of atomic degrees of freedom. Fig. 12(a) shows both the measured and predicted values of m using the topological constraint model (solid line) [25]. The experimental values of m obtained from viscosity measurements are in good agreement with the modeled fragility values.

Four types of bonding constraints are considered in the model: α) B–O and M^{NB}–O linear constraints; β) O–B–O angular constraints; γ) B–O–B angular constraints; and μ) additional modifier rigidity due to clustering effects. We note that the borate glasses are intrinsically hygroscopic and thus contain hydroxyl groups that are expected to break linear and angular constraints. This effect is not included in the current model, but the good agreement between data and model predictions of m suggests that neglecting the hydroxyl effect is a good approximation. Fig. 12 (b) shows the contribution of each type of constraint to the calculated fragility, i.e., it reveals the topological origins of fragility. The β constraints provide the largest contribution to fragility, while α and μ constraints have little influence on the fragility value. There are five β constraints per four-fold coordinated

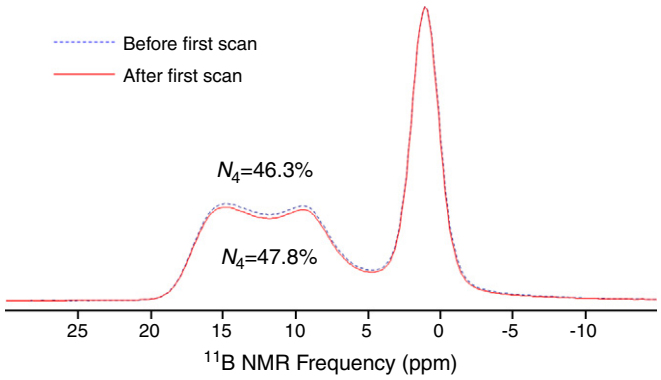

Fig. 13. ^{11}B MAS NMR spectrum of the glass with $x = 25$ (Fe-free) before and after first dynamic DSC scan at 20 K/min. The uncertainties in N_4 are on the order of $\pm 0.2\%$.

boron to form a rigid BO_4 tetrahedron and three β constraints per three-fold coordinated boron to keep the BO_3 unit planar [25]. Most importantly, fragility is a first-derivative property and the constraint onset temperature of β constraints is close to T_g. Therefore, the derivative of β constraints is large, and these constraints therefore have a large contribution to fragility. Thus, the boron speciation substantially affects fragility.

The indirect measures of the thermodynamic fragility (i.e., $C_{p,peak}$–C_{pg} and glass transition width) both exhibit a positive correlation with kinetic fragility m. The $C_{p,peak}$–C_{pg} measurement is a reflection of both thermodynamics and kinetics, since higher fragility leads to a sharper and more well-defined glass transition [37] and the value of $C_{p,peak}$ is influenced by the kinetic glass transition process. Therefore, m has a positive relation with both $C_{p,peak}$–C_{pg} and the glass transition width.

An inverse correlation between fragility and GFA has been found for various metallic glasses [24,40], and hence fragility can be used as a quantitative measure of GFA for those systems. However, we find that this is not the case for these soda lime borate compositions. Comparing Fig. 12(a) with Fig. 11(a), we can see that fragility and GFA do not exhibit a linearly inverse relation. In addition, the thermodynamic fragility (shown in Figs. 6 and 7) and GFA also do not exhibit this relation. As mentioned above, both NBO/B and boron speciation affects the degree of network connectivity. Within different amounts of network former, NBO/B plays a determining role in controlling GFA, while the boron speciation plays a less important role for GFA. However, when we calculate the fragility with topological constraint theory, the boron speciation is counted, which plays a less important role for GFA in different compositions. In addition, GFA is related to many other properties, e.g., the degree of network connectivity [24], liquidus temperature [14,41], but it is not necessarily related to only fragility [40]. Therefore, GFA and m might not have a linear inverse correlation.

4.3. Enhancement of glass stability

Interestingly, the glass stability becomes enhanced for some of the glasses after the first DSC up- and downscans, as shown in Figs. 8 and 9. Now the question arises: what is the origin of the enhancement of the GS after slow cooling? To answer this question, we discuss several factors which could affect the crystallization behavior of these glasses.

For borate systems, liquid-liquid phase separation is often an issue to consider [42]. Phase separation could occur during the first DSC upscan, since phase separation is more favorable at higher temperatures due to the supplementation of thermal energy. Hence, the atoms more easily overcome the energy barriers to rearrange and favor phase separation [1]. If phase separation has occurred, there will be two glassy phases and during the second DSC upscan, the T_g and the C_p jump should have changed and a second glass transition peak should have been observed. However, we did not observe these changes and we therefore exclude this factor. Moreover, the enhancement of GS is likely not attributed to the evaporation of boron during the DSC scans. Boron vaporizes rapidly when the temperature is above 1473 K [43], but the sample was only scanned to 1273 K, and therefore the temperature was low enough to exclude significant boron evaporation. Another possible explanation could be that during the first upscan, the glass disk was inserted in the Pt crucible with relatively poor contact between glass and Pt crucible. However, during the second upscan, the sample stuck to the Pt-crucible due to the melting during the first upscan. The heat transfer was then more efficient during the second upscan, since there is minimal air gap between the sample and the bottom of the Pt crucible. In order to explore this possible explanation for a change in GS, we melted the glass inside the Pt-crucible in the induction furnace and then performed the DSC scan. We observed the same phenomenon, i.e., the enhancement of GS first occurs during the second upscan. Thus, we can also exclude any effects related to the surface contact between glass and crucible.

Instead, the enhancement of GS might be related to the temperature dependence of the boron speciation. Temperature-induced changes in boron speciation have been reported in alkali borate glasses and melts [44,45]. According to these previous studies, the fraction of BO_4 tetrahedra decreases with increasing temperature above T_g, indicating that the BO_4 tetrahedra in the glass are converted to BO_3 triangles in the melt [44]. The BO_4 to BO_3 conversion can lower the rigidity of the glasses, since the degree of cross-linking of the borate framework with covalent B–O bonds is lowered [44]. According to [25], there are five β constraints (O–B–O angular constraints) per B^4 to form a rigid BO_4 tetrahedron and three β constraints per B^3 to keep the BO_3 unit planar. Thus, the glass containing more BO_3 has a less rigid network structure. In other words, the degrees of freedom of the liquid at the crystallization temperature increase with increasing BO_3 concentration. This facilitates rearrangement of the structural units, and hence crystallization. Consequently, the glass stability is lowered. In Section 4.1 we mentioned that in glasses with different amount of network former, NBO/B plays a determining role in controlling GFA, while the boron speciation plays a less significant role. However, considering a constant concentration of network former, the boron speciation conversion will have a significant effect. An increase of N_4 after the first upscan will result in a decrease of NBO, which is expected to cause an increase of GS. Therefore, this combination of two effects should lead to a substantially enhanced GS.

The concentrations of BO_3 and BO_4 in a borate glass depend on the cooling rate that the borate melt experienced during production, i.e., its thermal history [46–49]. The GFA is ultimately determined during this cooling process. The as-produced glasses studied here have been subjected to a relatively fast cooling (approximately 1000 K/s [50]). After the first DSC upscan, the melt was cooled at a slower rate, i.e., 0.17 K/s. The higher the cooling rate, the higher fraction of BO_3 is frozen-in. Upon re-heating, the rapidly cooled glass should crystallize more easily than the slowly cooled glass due to the factors mentioned above. In order to test whether these inferences are reasonable, ^{11}B MAS NMR measurements have been conducted on the Fe-free glass (B-Na25) before and after the first upscan. We choose an iron-free analogous glass in order to avoid the effect of dipolar coupling between ^{11}B nuclear spin and unpaired spin of d-electrons in Fe during the NMR measurement. As shown in Fig. 13, the N_4 values for the glass before and after the first upscan are 46.3 and 47.8 at%, respectively. For relatively fast cooling (before first upscan), more BO_3 species are frozen-in and the N_4 value is low. For a slower cooling (after first upscan), less BO_3 species are frozen-in and N_4 attains a higher value. N_4 increases by 1.5 at% after the first up- and downscans. This provides evidence for the possible link between the boron speciation and the enhanced GS.

5. Conclusions

The glass forming ability (GFA) of a series of soda lime borate liquids has been determined using a calorimetric method. Specifically, we express GFA in terms of the Hruby parameter. It is found that GFA decreases when Na_2O is substituted for B_2O_3, implying that the network connectivity greatly controls GFA of the studied systems. We note that the applicability of the Hruby parameter is limited only to the poor glass formers. The inverse correlation between liquid fragility and GFA, which has been found for some glass-forming liquid series, is not observed for these systems. We also report a remarkable result concerning the stability of two glasses, containing 20 and 25 mol% Na_2O, against crystallization. Their GS during heating is enhanced when the glasses have previously been subjected to a relatively slow cooling cycle, e.g., a 10–20 K/min cooling rate. This enhancement of GFA can be attributed to the structural conversion of BO_3 units into BO_4 units during this slow cooling process. This conversion increases the network connectivity of the glass, and hence the GFA.

Acknowledgments

We thank Mette Moesgaard for performing the XRD measurements and Ralf Keding for valuable discussions.

References

[1] J.E. Shelby, Introduction to Glass Science and Technology, second Ed. The Royal Society of Chemistry, 2005.
[2] A.K. Varshneya, Fundamentals of Inorganic Glasses, Academic, 1994.
[3] C.A. Angell, Science 267 (1995) 1924.
[4] A.A. Cabral Jr., C. Fredericci, E.D. Zanotto, J. Non-Cryst. Solids 219 (1997) 182.
[5] M.L.F. Nascimento, L.A. Souza, E.B. Ferreira, E.D. Zanotto, J. Non-Cryst. Solids 351 (2005) 3296.
[6] I. Avramov, E.D. Zanotto, M.O. Prado, J. Non-Cryst. Solids 320 (2003) 9.
[7] A.A. Soliman, I. Kashif, Phys. B 405 (2010) 247.
[8] P. Wray, Am. Ceram. Soc. Bull. 90 (2011) 25.
[9] J.C. Mauro, P.K. Gupta, R.J. Loucks, J. Chem. Phys. 130 (2009) 234503.
[10] T. Wakasugi, R. Ota, J. Fukunaga, J. Am. Ceram. Soc. 75 (1992) 3129.
[11] Z.P. Lu, C.T. Liu, Phys. Rev. Lett. 91 (2003) 11505.
[12] A. Hruby, Czech. J. Phys. B 22 (1972) 1187.
[13] E.B. Ferreira, M.L. Lima, E.D. Zanotto, J. Am. Ceram. Soc. 93 (2010) 3757.
[14] R. Ota, T. Wakasugi, W. Kawamura, B. Tuchiya, J. Fukunaga, J. Non-Cryst. Solids 188 (1995) 136.
[15] F. Stickel, E.W. Fischer, R. Richert, J. Chem. Phys. 102 (1995) 6251.
[16] I. Avramov, A. Milchev, J. Non-Cryst. Solids 104 (1988) 253.
[17] J.C. Mauro, Y.Z. Yue, A.J. Ellison, P.K. Gupta, D.C. Allan, Proc. Natl. Acad. Sci. U. S. A. 106 (2009) 19780.
[18] P.K. Gupta, J.C. Mauro, J. Chem. Phys. 130 (2009) 094503.
[19] J.C. Phillips, J. Non-Cryst. Solids 34 (1979) 153.
[20] J.C. Phillips, M.F. Thorpe, Solid State Commun. 53 (1985) 699.
[21] Q.J. Zheng, J.C. Mauro, A.J. Ellison, M. Potuzak, Y.Z. Yue, Phys. Rev. B 83 (2011) 212202.
[22] Y.Z. Yue, J. Non-Cryst. Solids 354 (2008) 1112.
[23] R. Busch, E. Bakke, W.L. Johnson, Acta Mater. 46 (1998) 4725.
[24] M. Moesgaard, Y.Z. Yue, J. Non-Cryst. Solids 355 (2009) 867.
[25] M.M. Smedskjaer, J.C. Mauro, S. Sen, Y.Z. Yue, Chem. Mater. 22 (2010) 5358.
[26] M.M. Smedskjaer, J.C. Mauro, S. Sen, J. Deubener, Y.Z. Yue, J. Chem. Phys. 133 (2010) 154509.
[27] M.M. Smedskjaer, J. Deubener, Y.Z. Yue, Chem. Mater. 21 (2009) 1242.
[28] Y.Z. Yue, J. de C. Christiansen, S.L. Jensen, Chem. Phys. Lett. 357 (2002) 20.
[29] N. Böse, G. Klingenberg, G. Meerlender, Glass Sci. Technol. 74 (2001) 115.
[30] T.J. Kiczenski, L.S. Du, J. Stebbins, J. Non-Cryst. Solids 351 (2005) 3571.
[31] D. Massiot, F. Fayon, M. Capron, I. King, S.L. Calvé, B. Alonso, J. Durand, B. Bujoli, Z. H. Gan, G. Hoatson, Magn. Reson. Chem. 40 (2002) 70.
[32] K. Ito, C.T. Moynihan, C.A. Angell, Nature 398 (1999) 492.
[33] L.M. Wang, C.A. Angell, R.J. Richert, J. Chem. Phys. 125 (2006) 074505.
[34] D.H. Huang, G.B. McKenna, J. Chem. Phys. 114 (2001) 5621.
[35] J.C. Mauro, R.J. Loucks, Phys. Rev. E 78 (2008) 021502.
[36] M. Solvang, Y.Z. Yue, S.L. Jensen, D.B. Dingwell, J. Non-Cryst. Solids 351 (2005) 499.
[37] J.C. Mauro, D.C. Allan, M. Potuzak, Phys. Rev. B 80 (2009) 094204.
[38] J. Fayos, R.A. Howie, F.P. Glasser, Acta Crystallogr. C 41 (1985) 1394.
[39] J.F. Stebbins, Z. Xu, Nature 390 (1997) 60.
[40] X.F. Bian, J. Guo, X.Q. Lv, X.B. Qin, C.D. Wang, Appl. Phys. Lett. 91 (2007) 221910.
[41] C.A. Angell, J. Non-Cryst. Solids 354 (2008) 4703.
[42] W.F. Du, K. Kuraoka, T. Akai, T. Yazawa, J. Mater. Sci. 35 (2000) 4865.
[43] P.W. Angel, A.R. Cooper, J. Non-Cryst. Solids 221 (1997) 70.
[44] O. Majérus, L. Cormier, G. Calas, B. Beuneu, Phys. Rev. B 67 (2003) 024210.
[45] T. Yano, N. Kunimine, S. Shibata, M. Yamane, J. Non-Cryst. Solids 321 (2003) 147.
[46] S. Sen, J. Non-Cryst. Solids 253 (1999) 84.
[47] L. Cormier, O. Majérus, D.R. Neuville, G. Calas, J. Am. Ceram. Soc. 89 (2006) 13.
[48] J.F. Stebbins, S.E. Ellsworth, J. Am. Ceram. Soc. 79 (1996) 2247.
[49] J.S. Wu, M. Potuzak, J.F. Stebbins, J. Non-Cryst. Solids 357 (2011) 3944.
[50] Y.Z. Yue, R. von der Ohe, S.L. Jensen, J. Chem. Phys. 120 (2004) 8053; ibid. 121 (2004) 11508.